ELSEVIER

Powder Technology 82 (1995) 115–121

POWDER TECHNOLOGY

Theory of sound propagation in suspensions: a guide to particle size and concentration characterization

Harri K. Kytömaa

Failure Analysis Associates, Three Speen Street, Framingham, MA 01701, USA

Received 17 September 1994; in revised form 4 November 1994

Abstract

There has been recent increasing interest in the acoustic properties of suspensions for applications such as ultrasonic particle size and concentration instrumentation. This paper aims to summarize what is known about the acoustic properties of suspensions of solids in a liquid and aims to identify the methods that enable useful information to be extracted from sound speed and attenuation information such as particle size, concentration, and the mechanical properties of the constituents. The paper identifies regimes of sound propagation and present models for these that can be used for size characterization of slurries.

Keywords: Sound propagation; Particle size; Suspensions; Concentration

1. Introduction

The acoustic properties of heterogeneous media with a continuous fluid phase have been of interest in numerous applications, such as predicting the effectiveness of fog horns (water droplets in air) and describing the acoustics of bubbly and two-phase flows that are encountered in the process and the nuclear power generation industries. More recently there has been an increasing interest in the acoustic properties of suspensions for acoustic telemetry through drilling fluids, as well as a rising demand for ultrasonic particle size and concentration instrumentation. Commercial instruments have been developed to characterize the properties of suspensions using ultrasound (e.g., O'Brien [1]). This paper presents what is known about this subject in the specific context of suspensions of solids in a liquid and aims to identify the mechanisms that enable useful information to be extracted from sound speed and attenuation information such as particle size, concentration and the mechanical properties of the constituents.

Sound propagation through saturated porous media has also been of significant interest for the second half of this century in applications such as seismic sounding for geological imaging in both the petroleum and mineral industries, and more recently in nondestructive evaluation of composites such as ceramics, metal-matrix and the more conventional resin/fiber composites. Much of the ground-breaking work in the context of fluid-filled solids was done by Biot [2], who identified two longitudinal waves and a shear wave, each of different speed and attenuation. The faster longitudinal wave corresponds to in-phase compression of the fluid and the solid, and the slower to out-of-phase compression. The shear wave arises due to the shear stiffness of the skeletal solid medium, and these, as well as the slow compressional waves, disappear when the skeletal frame loses its shear and compressional stiffness. These three modes can only coexist when both the shear and bulk moduli of the skeletal frame are finite, and the permeability of the fluid is finite. In situations where any one of these conditions is violated, the number of possible modes decreases. For example, solids with closed pockets of fluids (zero fluid permeability), or fluids with suspended solids (zero skeletal shear and bulk moduli) do not exhibit this same complexity. Suspensions can only accommodate fast compressional waves.

2. Regimes of sound propagation in a suspension

Different regimes of compressional wave propagation can be identified on the basis of the dominant length scales of the process.

SSDI 0032-5910(94)02901-Y

2.1. The multiple-scattering regime (short wavelength regime $ka \gg 1$)

The most natural length scale for compressional wave propagation is the wavelength, λ, which is determined by the material properties and the frequency of emission. The parameter ka, where k is the wavenumber $2\pi/\lambda$ and a is the particle radius, represents the ratio of the particle dimension to the wavelength. When $ka \gg 1$, the particles are large compared to the wavelength, and sound scatters geometrically. In an assembly of many randomly arranged particles, sound will scatter randomly and will penetrate poorly. This is the multiple-scattering regime, for which it has been shown that the dimensionless attenuation αa, where $1/\alpha$ is the e-folding depth of penetration, scales with frequency to the fourth power. For the present purpose of ultrasonic diagnostics in suspensions, it is desirable to obtain good penetration, and the high attenuation of the multiple-scattering regime renders it undesirable; it is more effective to ensure that ka is not much greater than one. It will later be indicated that it is possible to size particles by identifying this transition.

2.2. The viscous regime

In the long wavelength regime, another natural length scale arises in the context of viscous fluids, namely the viscous boundary layer thickness, $\delta = \sqrt{2\mu/(\rho_l \omega)}$, surrounding the particles, also often called the Stokes layer thickness. The ratio of particle radius to δ constitutes a Reynolds number

$$\mathrm{Re} = \frac{a}{\delta} = a\sqrt{\rho_l \omega/(2\mu)} \tag{1}$$

also called the Womersley parameter in the context of oscillatory flow in arteries [3]. The square of this parameter has the more usual form of a Reynolds number based on $a\omega$ as the characteristic velocity. This has also been called the vibration number in the context of turbulence/particle interactions [4]. When $\mathrm{Re} \ll 1$, the boundary layer is thick compared to the particle radius, the viscous relaxation time is shorter than the period of excitation, and the drag is well represented by the Stokes law. In this regime the attenuation has been shown to scale with $a^2\omega^2/\mu$ [2].

2.3. The inertial regime

When $\mathrm{Re} \geqslant 1$, inertial effects become significant and the Basset history term begins to influence the particle drag. At $\mathrm{Re} \gg 1$, δ is very small, and the fluid outside the thin boundary layer is governed by inviscid inertial effects. Consequently, the drag becomes dominated by inertia through the added mass effect. However, the added mass force is conservative and does not contribute to losses, and the dominant loss term is the in-phase component of the Basset force. Therefore it cannot be neglected in any model that attempts to capture attenuation. In this regime, the attenuation has been shown to scale with $(\mu\omega)^{1/2}/a$ [2].

3. Other effects

Submerged particles may exhibit resonant characteristics, and the period of the first mode of resonance can be approximated by the time sound takes to travel twice the diameter of the particle. Higher modes will have periods that are integral fractions of the first. In practice, materials such as silica or other minerals tend to have sound speeds sufficiently elevated so that the multiple-scattering transition will set in first. However, most plastics will often exhibit resonant absorption at frequencies below the $ka = 1$ threshold [5,6] which result in very large attenuations over a narrow band of frequencies.

In situations where either the continuous fluid or the dispersed phase is a gas, thermal effects can come into play. At sufficiently low frequencies, thermal equilibration will occur on a time scale shorter than the period of oscillation, and the systems will behave in an isothermal fashion. At sufficiently elevated frequencies, a thin unsteady thermal boundary layer forms in the gas and the bulk of the gas essentially behaves adiabatically. Unsteady thermal conduction can be a significant source of attenuation [7]. The governing dimensionless parameter is the ratio of the particle size to the thermal boundary layer thickness a/δ_{th}, which is the above Reynolds number multiplied by $\sqrt{\mathrm{Pr}}$, where $\mathrm{Pr} = \nu/\alpha$ and α is the thermal diffusivity. The combination Re Pr is also often called the Peclet number. As this article addresses liquid–solid systems, these effects are small and will not be discussed further.

4. Regime map

The Reynolds number therefore separates the viscous (low Re) and the inertial (high Re) regimes, while $ka > 1$ identifies the onset of the multiple-scattering regime. For a given pair of materials such as silica and water, which are representative of numerous mineral processes, one can draw a regime map on the basis of the material bulk moduli and densities, as shown in Fig. 1. With increasing frequency, regime transitions for particle sizes greater than 0.1 mm arise in the order viscous to inertial to multiple-scattering, while for smaller particles, the viscous regime gives way to multiple-scattering before inertial effects become important. Thus, the pure inertial regime only exists for particles bigger than 10 μm. The two transitions associated with

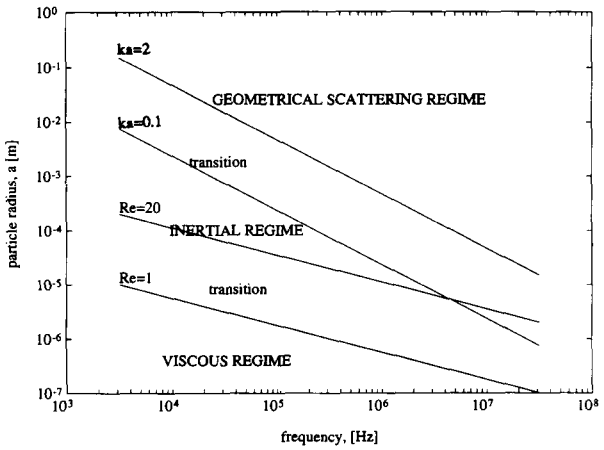

Fig. 1. Map of regimes of sound propagation through a suspension of silica in water. In order of increasing frequency, these are the viscous, the inertial and the geometric scattering regimes. Note that the inertial regime ceases to exist for sufficiently small particles ($a<10$ μm).

the relation between particle size and the relevant length scales represent a change in the attenuation scaling. Therefore by identifying such a change in the scaling, it is possible to determine particle size, as has been demonstrated by Riebel and Löffler [8] and Salin and Schön [9], for example. For large particles (>10 μm) the two transitions provide double the information; this can be beneficial for robust sizing purposes as it provides redundancy to the measurement. To the author's knowledge, these two transitions have not yet been used in combination to improve the quality of inferred particle size.

5. Theoretical prediction of sound speed and attenuation

Most models used to infer solids concentration from attenuation tend to assume that these are linearly related, which in practice is reasonable only up to concentrations of around 10%. At higher concentrations particle interactions become significant, as has been well documented in the concentration-dependent hindered motion of particle assemblies in a viscous fluid at low Re (e.g. Zick and Homsy [10], Richardson and Zaki [11]), or the concentration-dependent added mass coefficient that reflects inviscid interactions between particles at high Re [12]. In this section, rather than develop theories that have been presented elsewhere, the present aim is to identify the elements that are generally accepted and those that are either still contested or not known.

In the long wavelength limit, an effective approach has been to describe the fluid and the solids as two interacting continua. Both constituents are assumed to compress isotropically and their compressibility is described by means of an equation of state for each component, the mass of which is conserved using a continuity equation. The dynamics of the two components are described through two coupled momentum equations. The coupling term describes the force exerted by one component on the other, and it appears in both equations in an equal but opposite sense.

Two formulations of different disciplinary origins exist. In the porous medium literature, the force interaction term is represented through the dynamic permeability [13–18] while the two-phase flow literature uses a dynamic drag originally due to Landau and Lifshitz [19]. These are essentially equivalent [20,21], and reflect the same viscous and inertial asymptotic limits. The suspension formulation is only briefly described as it is presented in detail elsewhere [e.g. 21]. For low amplitude harmonic excitation of an assembly of spheres in a fluid, we denote the one-dimensional relative velocity by $U_{rel}=v_s-v_l=U_0e^{i\omega t}$, where v_s is the instantaneous solid velocity and v_l is defined as $j_l/(1-\nu)$ where j_l is the instantaneous superficial liquid velocity, also called the liquid volume flux. The resulting force per sphere required to sustain this motion is $F_De^{i\omega t}$ where F_D is generally complex. For small amplitude oscillations free of boundary layer separation,

$$F_D=6\pi\mu aU_0\left[f(\nu)+\frac{a}{\delta}(1+i)+i\left(\frac{a}{\delta}\right)^2\frac{4}{9}C(\nu)\right] \quad (2)$$

F_D consists of three terms of increasing order in Reynolds number. The first is the hindered Stokes drag, the second the history-dependent Basset force and the third is the added mass term. As Re is increased from a small value, each becomes dominant in turn in the order stated. At $Re\ll 1$, Stokes drag dominates. $f(\nu)$ is the concentration-dependent viscous drag coefficient, which has been extensively studied. For our purposes it is sufficient to use the Richardson and Zaki [11] model, which satisfactorily captures the full range of ν:

$$f(\nu)=\frac{1}{(1-\nu)^{n-2}} \quad (3)$$

where $n=4.65$ for $a<10$ μm. At $Re\approx 1$, the Basset term assumes the same order of magnitude as the Stokes drag, and introduces an out-of-phase (conservative) component to the force. As $Re\to\infty$, the added mass term becomes dominant, although it is important to recognize that this effect is conservative, and the leading dissipative mechanism remains viscous through the $O(a/\delta)$ real component of the Basset force.

Particle–particle interactions are depicted by the concentration dependence in the added mass coefficient at high Re. Current theory is only able to predict added mass to first order in solid fraction:

$$C(\nu)=\frac{1}{2}(1+3.32\nu)+O(\nu^2) \tag{4}$$

which is only valid for low concentrations (see for example Refs. [12,22–25]). This term remains the subject of heated discussion, and careful experiments and numerical simulations appear most promising as a means of determining the form of $C(\nu)$ at high values of ν. Furthermore, for transition conditions where $\mathrm{Re}\approx 1$, the concentration dependence of the Basset force is unknown, and it can only be presented in the isolated particle form.

With this mathematical framework, we now seek traveling wave solutions of the form

$$q=q_0 e^{i(\omega t+kx)} \tag{5}$$

where k is the complex wavenumber

$$k=\frac{\omega}{c}+i\alpha \tag{6}$$

c is the wave speed in the medium and α is the spatial attenuation parameter. Upon linearization, the described system of equations [21] yields the following expression for k:

$$k^2=\frac{\omega^2}{\bar{\kappa}}\frac{[(A+i\omega B)\bar{\rho}+i\omega\rho_s\rho_l(1-\nu)]}{A+i\omega B+i\omega(1-\nu)\rho^*} \tag{7}$$

The variables $\bar{\kappa}$ and $\bar{\rho}$ denote the effective medium bulk modulus and density respectively:

$$\frac{1}{\bar{\kappa}}=\frac{\nu}{\kappa_s}+\frac{(1-\nu)}{\kappa_l} \tag{8}$$

and

$$\bar{\rho}=\nu\rho_s+(1-\nu)\rho_l \tag{9}$$

The quantities ρ^*, A and B are defined as

$$\rho^*=(1-\nu)\rho_s+\nu\rho_l \tag{10}$$

$$A=\frac{9\mu}{2a^2}\left(f(\nu)+\frac{a}{\delta}\right) \tag{11}$$

and

$$B=\rho_l\left[C(\nu)+\frac{9}{4}\frac{\delta}{a}\right] \tag{12}$$

The phase speed c is given by

$$c=\frac{\omega}{\mathcal{R}(k)} \tag{13}$$

and the attenuation

$$\alpha(\omega)=\mathcal{I}(k) \tag{14}$$

where $\mathcal{R}()$ and $\mathcal{I}()$ denote the real and imaginary parts of the argument.

The above equations can directly be used to compute the sound speed and attenuations for the full range of relevant frequencies. For practical purposes it is also useful to evaluate the asymptotic behavior of the sound speed and attenuation in the limits of $\omega\to\infty$ and $\omega\to 0$.

5.1. Sound speed

The low-frequency limit for the sound speed as predicted by the two component model is given by:

$$\lim_{\omega\to 0} c=\left(\frac{\bar{\kappa}}{\bar{\rho}}\right)^{1/2} \tag{15}$$

where $\bar{\kappa}$ and $\bar{\rho}$ are respectively the effective bulk modulus and density of the mixture. In this limit the sound speed reduces to that predicted by the phenomenological model of Urick [26]. The high-frequency limit for the sound speed is given by:

$$\lim_{\omega\to\infty} c=\left(\frac{\bar{\kappa}}{\bar{\rho}}\right)^{1/2}\left\{\frac{(C+(1-\nu)\rho^*/\rho_l)}{(C+(1-\nu)\rho_s/\bar{\rho})}\right\}^{1/2} \tag{16}$$

It is noteworthy that the sound speed is entirely independent of the fluid viscosity, while the criterion which determines the regime, Re, is.

The sound speed assumes two asymptotic forms which correspond to the viscous and the inertial regimes, as shown in Fig. 2. Both of these are independent of frequency (McClement and Povey [27]) and Fig. 3 indicates that the transition from one to the other occurs at $1<\mathrm{Re}<10$. The viscous curve exhibits a minimum, while the inertial one does not. This is of practical importance as there is a range of ambiguity associated with having two concentrations that can result in the same sound speed, if the latter is used to infer

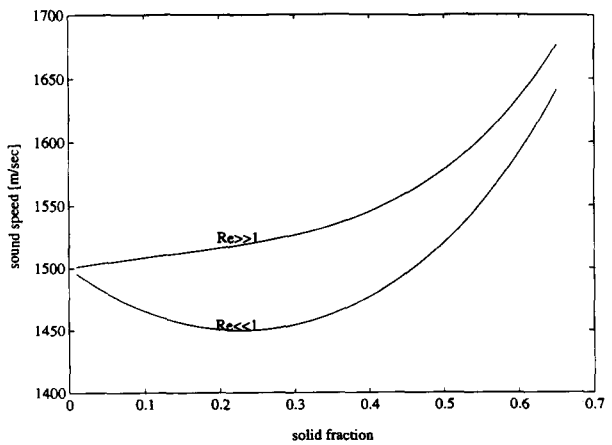

Fig. 2. Sound speed for a silica/water suspension as a function of solid fraction. The viscous and inertial limiting cases are shown. In the viscous regime, the sound speed assumes a minimum with respect to solid fraction, while it is monotonic in the inertial regime.

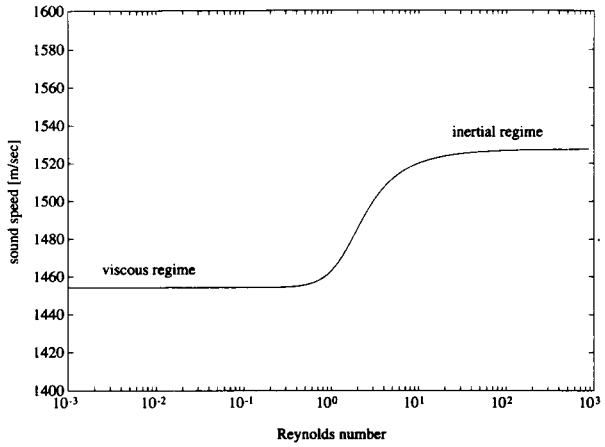

Fig. 3. Sound speed for a silica/water suspension at a solid fraction ν of 0.3, showing the transition from the viscous to the inertial regime in the range $1 < \mathrm{Re} < 10$.

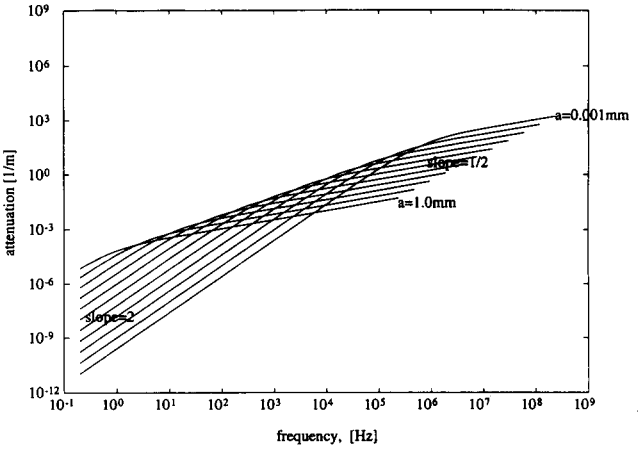

Fig. 4. Attenuation, α, shown as a function of frequency for different silica particle sizes suspended in water at $\nu = 0.3$. At the high frequency end the curves are truncated at $ka = 1$, which denotes the onset of the geometric scattering regime. The transition in the frequency dependence from f^2 to $f^{1/2}$ depends on particle size.

ν. This difficulty does not arise in the inertial regime as shown in Fig. 9.

5.2. Attenuation

In the low-frequency limit where viscous effects dominate, the attenuation is predicted to be:

$$\lim_{\omega \to 0} \alpha = \frac{a^2\omega^2}{9\mu}\left(\frac{\bar{\rho}}{\bar{\kappa}}\right)^{1/2}(\rho_s\rho_l/\bar{\rho} - \rho^*)\frac{(1-\nu)}{f(\nu)} \tag{17}$$

and it is found to be proportional to ω^2. It is interesting to observe that in the viscous regime, attenuation of sound scales inversely with viscosity, which suggests that at low frequencies, good penetration can readily be achieved with pastes and other thick mixtures.

At high frequencies the attenuation is given by:

$$\lim_{\omega \to \infty} \alpha = \frac{9}{4a}\sqrt{\frac{\mu\omega}{2\bar{\kappa}}} \times \frac{(1-\nu)(\rho_s\rho_l - \rho^*\bar{\rho})}{[\bar{\rho}C + \rho_s(1-\nu)]^{1/2}[\rho_l C + \rho^*(1-\nu)]^{3/2}} \tag{18}$$

This leads to the result that the attenuation is proportional to $(\mu\omega)^{1/2}$, which is consistent with the Biot theory [2]. It should be noted that here attenuation is due to the Basset or history terms that dominate drag losses at high frequencies of oscillation.

For small particle sizes (< 10 μm) and $ka < 1$, sound will propagate in the viscous regime.

5.2.1. Effect of frequency

Unlike the sound speed, the attenuation is dependent on the frequency and obeys a different scaling for each regime: ω^2, $\omega^{1/2}$, ω^4 for the viscous, the inertial and the geometric scattering regimes respectively. The first two are depicted in Fig. 4 and confirmed experimentally in Fig. 8. For particles greater than 10 μm, the two

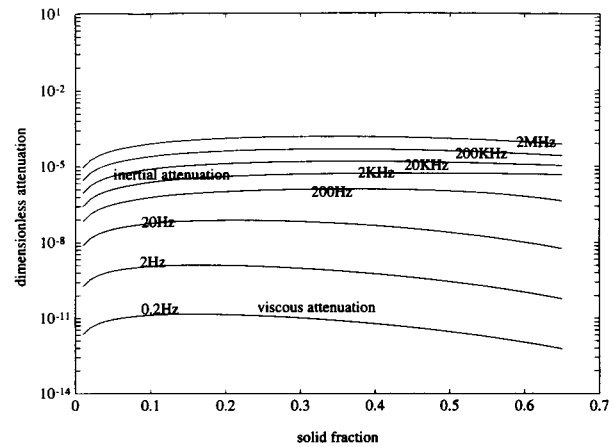

Fig. 5. Dimensionless attenuation, αa, shown as a function of solid fraction for $a = 100$ μm. In both regimes, the attenuation is far from linearly dependent on solid fraction, as is often assumed, and it exhibits a maximum at an intermediate concentration.

regime transitions can be used effectively to help in particle sizing. For smaller particles, the viscous regime gives way to the geometric scattering regime before inertial effects become important.

5.2.2. Effect of concentration

The sensitivity of attenuation to concentration is grossly nonlinear, as is depicted in Fig. 5. For a given frequency and size, it assumes a maximum at approximately 30%, and falls off at higher concentrations. As doubling the concentration does not double the attenuation, linear models that superimpose the contributions of different particle size groups fail at $\nu > 0.1$. Using guidance from the model presented here or other nonphysical means (e.g. [28,29]) such as neural nets and other sophisticated empirical correlation ap-

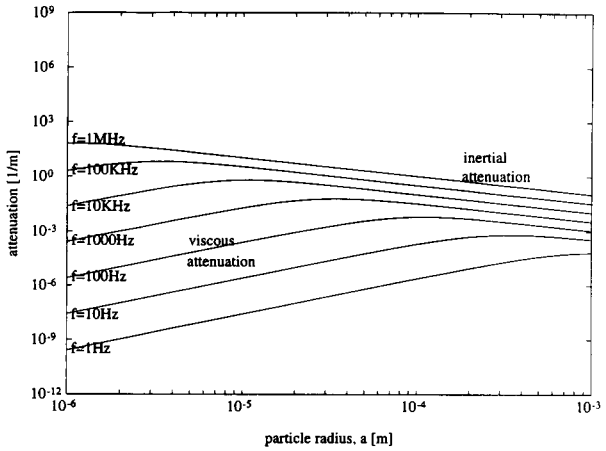

Fig. 6. The attenuation, α, is shown for $\nu = 0.3$ as a function of particle size. These curves show how attenuation increases with particle size in the viscous regime (a^2), while it decreases in the inertial regime (a^{-1}). Thus, particle sizes that correspond to $\mathrm{Re} = 1$ tend to contribute most to attenuation.

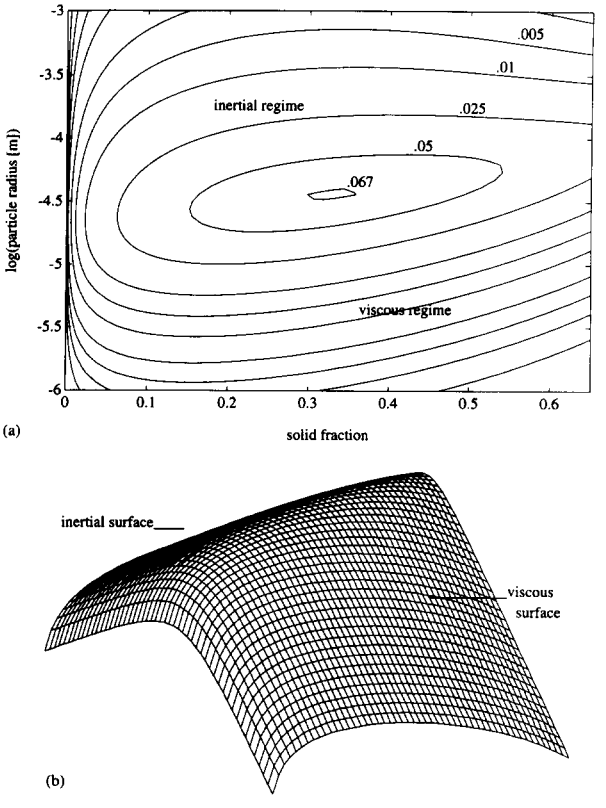

Fig. 7. (a) Contours of constant attenuation at $f = 1000$ Hz for various particle sizes and concentrations. This shows that an infinity of (ν, a) pairs, depicted by rings in this contour map, can yield a single attenuation value. (b) Attenuation surface for the same conditions. The attenuation and the particle size axes are logarithmic, thereby revealing the 'roof-top'-like constant slope dependence of attenuation with particle size seen in Fig. 6.

proaches, it is readily possible to construct the necessary nonlinear algorithms to determine size distribution.

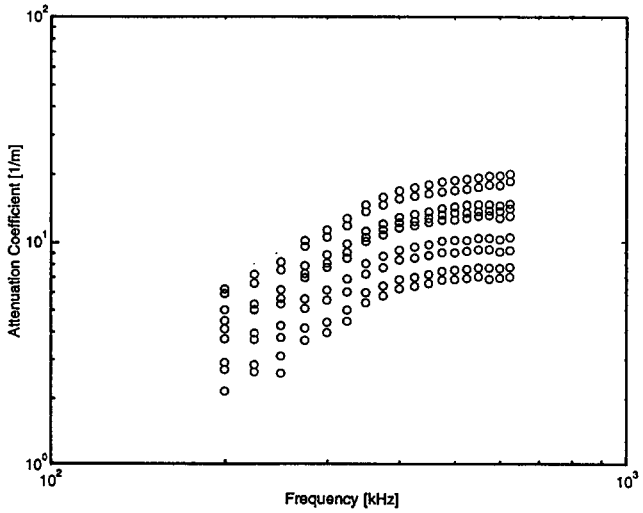

Fig. 8. Attenuation for a suspension of lead glass spheres (radius 50% within 24 μm $\pm$ 6 μm, $\rho_s = 2.83$ kg/m^3) for solid fractions of 0.58, 0.56, 0.49, 0.45, 0.39, 0.34, 0.30 and 0.26 in order of decreasing attenuation. The transition from the viscous to the inertial regime is reflected by a change in the slope from 2 to 1/2.

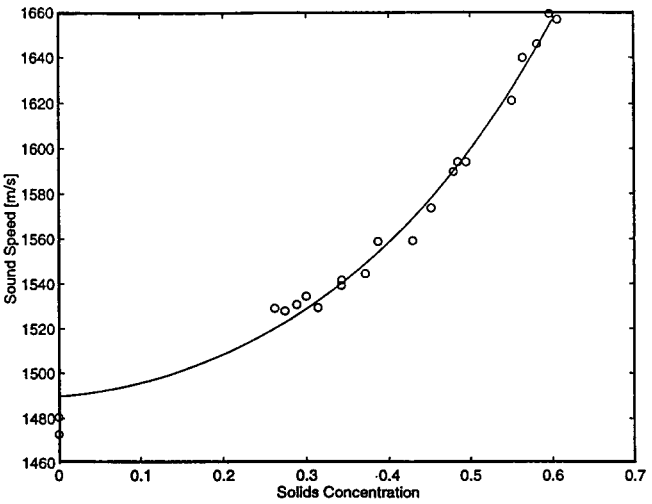

Fig. 9. Sound speed within the suspension of nominally 24 μm radius lead glass spheres in water. These measurements were conducted within the inertial regime at 450 kHz, as confirmed by Fig. 8. The monotonic rise is consistent with Fig. 2 and McClement and Povey [27]. The solid line is the corresponding theoretical prediction with $C(\nu) = \frac{1}{2}(1-\nu)^2$.

5.2.3. *Effect of particle size*

Eqs. (17) and (18) indicate that the attenuation is proportional to a^2 and a^{-1} in the viscous and inertial regimes respectively. It is shown in Fig. 6 (for $\nu = 0.3$) to assume a maximum around transition. In practice this implies that at a fixed ν particles whose size corresponds to $\mathrm{Re} \approx 1$ will contribute more to the attenuation than others, with the exception of those particles that are sufficiently large to satisfy $ka > 1$, for which $\alpha \propto a^3$.

To determine the particle size distribution of a suspension, it is useful to understand how different size

groups contribute to the attenuation as a function of the solid content in each group. Fig. 7(a) shows a map of equal spatial attenuation contours at $f=1000$ Hz as a function of both size and concentration. The same data are also shown in Fig. 7(b) as an attenuation surface. It is clear from these plots that there is an infinity of (ν, a) ordered pairs associated with each value of attenuation at a given frequency, unless it happens to correspond to the maximum of the shown surface. Therefore any reasonable attempt at sizing that is based on attenuation measurements must rely on a spectroscopic approach in which the medium is interrogated with numerous frequencies.

6. Conclusions

The greatest modeling challenges previously arose in the transitional regimes in which sound propagation characteristics could not be modeled well. The present theory can smoothly capture the viscous to inertial transition in the frequency domain and it has been shown to agree well with data due to Urick [26] and Hampton [30] which straddle the viscous and inertial regimes. Similarly, the present model is not limited to infinitesimal solid fractions, and can readily describe suspensions up to maximum packing concentrations.

The behavior of sound speed and attenuation in the long wavelength regimes can be summarized in the following terms:

Sound speed depends on material bulk stiffness, density and ν, and, in the asymptotic regimes, is independent of frequency, fluid viscosity and particle size. In the viscous regime, sound speed assumes a minimum with respect to ν, while it rises continually in the inertial regime. Unlike the sound speed, the attenuation strongly depends on frequency, fluid viscosity and particle size. In the viscous regime attenuation assumes the form:

$$\lim_{\omega\to 0}\alpha=\frac{a^2\omega^2\rho_l}{\mu}\left(\frac{\bar{\rho}}{\bar{\kappa}}\right)^{1/2} g(\nu,\ \rho_s/\rho_l)$$

where g is a known function. In the inertial regime the corresponding form is:

$$\lim_{\omega\to\infty}\alpha=\sqrt{\frac{\mu\omega}{a^2\bar{\kappa}}}\,h(\nu,\ \rho_s/\rho_l)$$

where h is also known.

While the present theory provides the scaling laws, an empirical calibration that covers the three regimes is necessary to arrive at relationships that can be used for size characterization.

The present overview clearly indicates that speed and attenuation each contain complementary information. Measurements that can make use of both are likely to be more robust.

Acknowledgements

The author gratefully acknowledges the generous support of Intevep, The Research and Technological Center of Petroleós de Venezuela and the National Science Foundation under Grant CTS-9107449.

References

[1] R.W. O'Brien, NIST Special Publication 856, 1993, *US Patent 5 059 909* (22 Oct. 1991).
[2] M. Biot, *J. Acoust. Soc. Am., 28* (1956) 179–191.
[3] J.R. Womersley, *J. Physiol., 127* (1955) 553–563.
[4] A.M. Al Taweel and J. Landau, *Int. J. Multiphase Flow, 3* (1977) 241–251.
[5] L. Schwartz and T.J. Plona, *J. Appl. Phys., 55* (1984) 3971–3977.
[6] J. Liu, D.A. Weitz and P. Sheng, *Phys. Rev. Lett., 65* (1990) 2602–2605.
[7] M.S. Plesset and A. Prosperetti, *Ann. Rev. Fluid Mech., 9* (1977) 145–185.
[8] U. Riebel and F. Löffler, *Chem. Eng. Technol., 12* (1989) 433–438.
[9] D. Salin and W.J. Schön, *J. Phys. Lett. (France), 42* (1981) 42.
[10] A.A. Zick and G.M. Homsy, *J. Fluid Mech., 115* (1982) 13–26.
[11] J.F. Richardson and W.N. Zaki, *Trans. Inst. Chem. Eng., 32* (1954) 35–53.
[12] G.B. Wallis, *Multiphase Sci. Technol., 5* (1989) 239–361.
[13] D.L. Johnson, J. Koplik and R. Dashen, *J. Fluid Mech., 176* (1987) 379–402.
[14] D.L. Johnson, T.J. Plona and C. Scala, *Phys. Rev. Lett., 49* (1982) 1840–1844.
[15] E. Charlaix, A.P. Kushnick and J.P. Stokes, *Phys. Rev. Lett., 61* (1988) 1595–1598.
[16] P. Sheng and M. Zhou, *Phys. Rev. Lett., 61* (1988) 1591–1594.
[17] M.-Y. Zhou and P. Sheng, *Phys. Rev. B, 39* (1989) 12027–12039.
[18] D.M.J. Smeulders, R.L.G.M. Eggels and M.E.H. van Dongen, *J. Fluid Mech., 245* (1992) 211–228.
[19] L.D. Landau and E.M. Lifshitz, *Fluids Mechanics*, Pergamon, Oxford, 16th edn., 1992, p. 95.
[20] B. Yavari and A. Bedford, *Int. J. Multiphase Flows, 16* (1990) 885–897.
[21] C.M. Atkinson and H.K. Kytömaa, *Int. J. Multiphase Flows, 18* (1992) 577–592; C.M. Atkinson and H.K. Kytömaa, *J. Fluids Eng., 115* (1993) 665–675; H.K. Kytömaa and C.M. Atkinson, *Mech. Mater.*, accepted for publication.
[22] N. Zuber, *Chem. Eng. Sci., 19* (1964) 897.
[23] L. Van Wijngaarden, *J. Fluid Mech., 77* (1976) 27–44.
[24] J.A. Geurst, *Physica, 129* (1985) 233.
[25] A. Bieusheuvel and S. Spoelstra, *Int. J. Multiphase Flow, 15* (1989) 911–924.
[26] R.J. Urick, *J. Acoust. Soc. Am., 18* (1947) 983–987.
[27] D.J. McClement and J.W. Povey, *Advances in Colloid Interfaces Sci., 27* (1987) 285–316.
[28] F. Alba, R. Davies, T. Allen and A. Boxman, *Engineering Foundation Workshop on the Control of Particulate Processes, Santa Barbara, CA, USA,* 24–29 Jan. 1993.
[29] H.P. Pendse, *Engineering Foundation Workshop on the Control of Particulate Processes, Santa Barbara, CA, USA,* 24–29 Jan. 1993.
[30] L. Hampton, *J. Acoust. Soc. Am., 42* (1967) 882–890.